

Geophysical Research Letters

RESEARCH LETTER

10.1002/2017GL073663

Key Points:

- Phase behavior analysis for carbon dioxide and nitrogen gas coinjections into methane hydrate-bearing sediments
- Hydrate stability is a strong function of composition so a graphical analysis like those used in enhanced oil recovery is presented
- Nitrogen coinjection is necessary to successfully store carbon dioxide with methane exchange since nitrogen induces three-phase equilibrium

Supporting Information:

- Supporting Information S1
- Table S1

Correspondence to:

K. N. Darnell, kdarnell@utexas.edu

Citation:

Darnell, K. N., P. B. Flemings, and D. DiCarlo (2017), Subsurface injection of combustion power plant effluent as a solid-phase carbon dioxide storage strategy, *Geophys. Res. Lett.*, 44, 5521–5530, doi:10.1002/2017GL073663.

Received 2 APR 2017 Accepted 24 MAY 2017 Accepted article online 30 MAY 2017 Published online 11 JUN 2017

Subsurface injection of combustion power plant effluent as a solid-phase carbon dioxide storage strategy

K. N. Darnell^{1,2}, P. B. Flemings^{1,2}, and D. DiCarlo³

¹Department of Geological Sciences, Jackson School of Geosciences, University of Texas at Austin, Austin, Texas, USA, ²Institute for Geophysics, Jackson School of Geosciences, University of Texas at Austin, Austin, Texas, USA, ³Department of Petroleum and Geosystems Engineering, University of Texas at Austin, Austin, Texas, USA

Abstract Long-term geological storage of CO_2 may be essential for greenhouse gas mitigation, so a number of storage strategies have been developed that utilize a variety of physical processes. Recent work shows that injection of combustion power plant effluent, a mixture of CO_2 and N_2 , into CH_4 hydrate-bearing reservoirs blends CO_2 storage with simultaneous CH_4 production where the CO_2 is stored in hydrate, an immobile, solid compound. This strategy creates economic value from the CH_4 production, reduces the preinjection complexity since costly CO_2 distillation is circumvented, and limits leakage since hydrate is immobile. Here we explore the phase behavior of these types of injections and describe the individual roles of H_2O , CO_2 , CH_4 , and N_2 as these components partition into aqueous, vapor, hydrate, and liquid CO_2 phases. Our results show that CO_2 storage in subpermafrost or submarine hydrate-forming reservoirs requires coinjection of N_2 to maintain two-phase flow and limit plugging.

1. Introduction

Hydrates, or hydrate clathrates, are nonstoichiometric, ice-like solid compounds that form at low temperatures and high pressures [$Sloan\ and\ Koh$, 2007]. The hydrate unit cell consists of hydrogen-bonded H₂O molecules organized as cages of various sizes and structures that enclose gas molecules, called guest molecules [$Sloan\ and\ Koh$, 2007]. Simple hydrates are composed of a single guest molecule (e.g., CH_4 hydrate, CO_2 hydrate, and H₂S hydrate), while mixed hydrates are composed of multiple guest molecules. On Earth CH_4 hydrates form in sediment buried below the seafloor throughout the world's oceans and below permafrost in the arctic [$Wallmann\ et\ al.$, 2012; Milkov, 2004]. Mixed hydrates of CH_4 and heavier hydrocarbons likely form where natural gas buoyantly ascends towards the seafloor [$Smith\ et\ al.$, 2014; $Paganoni\ et\ al.$, 2016], and mixed hydrates of CO_2 and CO_3 and CO_3 naturally form pipe-like structures on the seafloor near CO_3 vents [$Swart\ et\ al.$, 2000].

Hydrates provide ideal storage for gas molecules because they are dense, immobile solids. For example, massive deposits of naturally occurring CH_4 hydrates sequester CH_4 with an energy density exceeding that of natural gas for a suite of pressure-temperature conditions [Boswell and Collett, 2011]. For this reason, CH_4 production of hydrates is a possible future energy resource [Boswell, 2007], and significant research has been undertaken to understand how and where CH_4 hydrates could be produced [Collett et al., 2012; Moridis et al., 2007; Moridis and Reagan, 2011]. The natural storage potential of CH_4 hydrates motivated several hydrate-based CO_2 storage strategies [House et al., 2006; You et al., 2015; Sun and Englezos, 2017]. Storage of CO_2 as hydrate would limit fluid leakage into the surrounding environment [House et al., 2006] and would sequester the carbon for thousands of years [House et al., 2006]. While these strategies demonstrate CO_2 hydrate storage is possible in deep [House et al., 2006] or shallow [You et al., 2015] marine environments, they require injection of pure CO_2 and do not provide any useful by-product.

Hydrate-based "guest molecule exchange" is a technique in which fluid/gas injections into CH_4 hydrate-bearing reservoirs induce simultaneous CH_4 production and CO_2 storage [Ohgaki et al., 1996; Kang et al., 2014; Boswell et al., 2017]. The process exchanges CH_4 held in hydrate cages for the injected components resulting in CH_4 -enriched gas and mixed hydrate enriched in the injected gas [Park et al., 2006; Lee et al., 2013; Boswell et al., 2017]. Early work [Ohgaki et al., 1996; Ota et al., 2005a; Lee et al., 2003; Graue et al., 2008] suggested pure CO_2 injection because it is more stable than CH_4 as a hydrate former and because injection of additional

©2017. American Geophysical Union. All Rights Reserved.

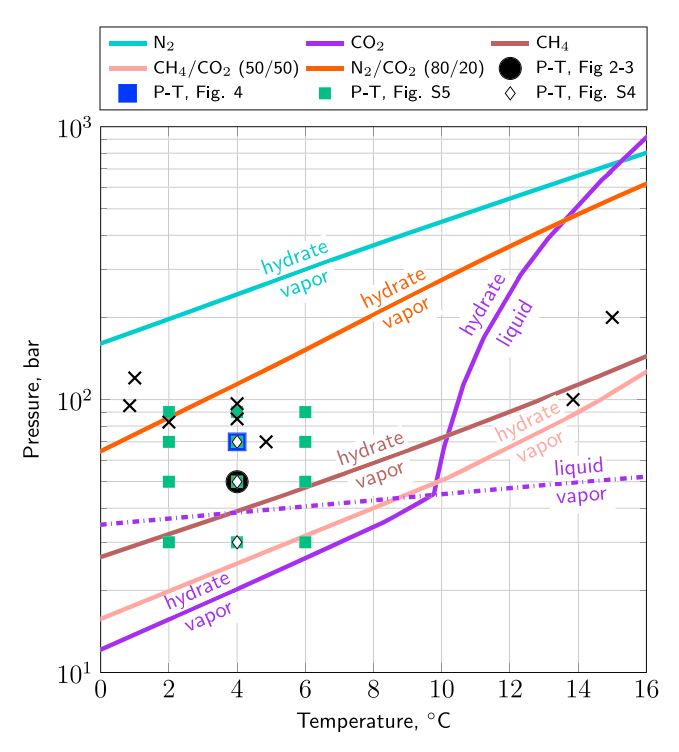


Figure 1. Pressure-temperature phase diagram for simple (single guest) hydrates, mixed hydrates (multiple guests), and vapor-liquid equilibrium of CO₂. Mixtures are reported in mole percent. Stable phases are labeled above and below phase boundaries. Colored markers indicate pressures and temperatures analyzed in subsequent figures. Black crosses designate experimental conditions reported in Table S1.

components could reduce $\mathrm{CO_2}$ storage capacity. However, evidence from the laboratory [Park et al., 2006; Birkedal et al., 2015; Seo et al., 2015] and the field [Schoderbek and Boswell, 2011; Boswell et al., 2017] shows that coinjections of $\mathrm{N_2}$ and $\mathrm{CO_2}$ such as combustion power plant effluent, or flue gas (i.e., 80 mol.% $\mathrm{N_2}$ and 20 mol % $\mathrm{CO_2}$), may be necessary to achieve exchange under water-rich field conditions, which conveniently circumvents pure $\mathrm{CO_2}$ distillation from flue gas.

However, fluid and heat flow models of multicomponent hydrate systems are currently primitive [White and Suk Lee, 2014; Anderson et al., 2014], so the dynamics within the interior of the reservoir are still ambiguous. At present, research on hydrate-based guest molecule exchange relies on effluent histories from core-scale experiments [Youn et al., 2016; Birkedal et al., 2015; Seo et al., 2015] using theoretical [Sun and Englezos, 2017; Birkedal et al., 2015] or experimental [Sun et al., 2016] mixed hydrate stability curves at specific compositional mixtures. For instance, effluent histories from laboratory

experiments demonstrate exchange is possible by injection of flue gas into sandstone cores [Birkedal et al., 2015], sand-packed columns [Seo et al., 2015; Yonkofski et al., 2016], and glass bead-packed columns [Youn et al., 2016]. Effluent histories from a field-scale production test on the northern Alaskan slope also show successful exchange from flue gas injection into a reservoir overlain by 500 m of permafrost [Schoderbek and Boswell, 2011; Boswell et al., 2017].

The exact mechanism responsible for the improved efficiency of flue gas injections over pure CO₂ injections is unclear [Kang et al., 2014; Koh et al., 2012; Birkedal et al., 2015]. In pure CO2 injections into water-limited systems, a solid-solid exchange process occurs in which hydrate cages remain intact as CH4 diffuses out of hydrate into the vapor and CO₂ diffuses out of vapor into the hydrate [Ota et al., 2005b]. In pure CO₂ injections into water-rich systems, excessive CO₂ hydrate formation restricts fluid flow and limits exchange [Birkedal et al., 2015]. The input of N₂ (or O₂) facilitates a thermodynamically favorable workaround to these issues [Kang et al., 2014; Birkedal et al., 2015] that is fundamentally different from pure CO₂ injections. Boswell et al. [2017] interpreted the field test results of flue gas injection as a "bulk exchange" of CH₄ for CO₂ that combined mixed hydrate formation with hydrate dissociation. Kang et al. [2014] similarly described coinjections as a "replacement and decomposition" process, while pure CO2 injections were exclusively a "replacement" process. The ambiguity of coinjection dynamics is compounded because pure N2 injections have also been invoked as a hydrate dissociation mechanism for hydrate-plugged pipelines in a method called "nitrogen purging" [Panter et al., 2011]. It is therefore unclear how coinjections of N₂ and CO₂ into water-rich CH₄ hydrate-bearing reservoirs result in bulk exchange of CO₂ for CH₄ or how the dynamics of a bulk exchange [Boswell et al., 2017] differ from original descriptions of solid-state "guest molecule exchange" [Ohgaki et al., 1996; Ota et al., 2005b].

To elucidate dynamical compositional changes that occur in mixed hydrate systems, we focus on the compositionally dependent thermodynamic stability of mixed and simple hydrates of $H_2O/CH_4/CO_2/N_2$ mixtures. We analyze the system using a pressure versus temperature phase diagram (Figure 1), compositional ternary

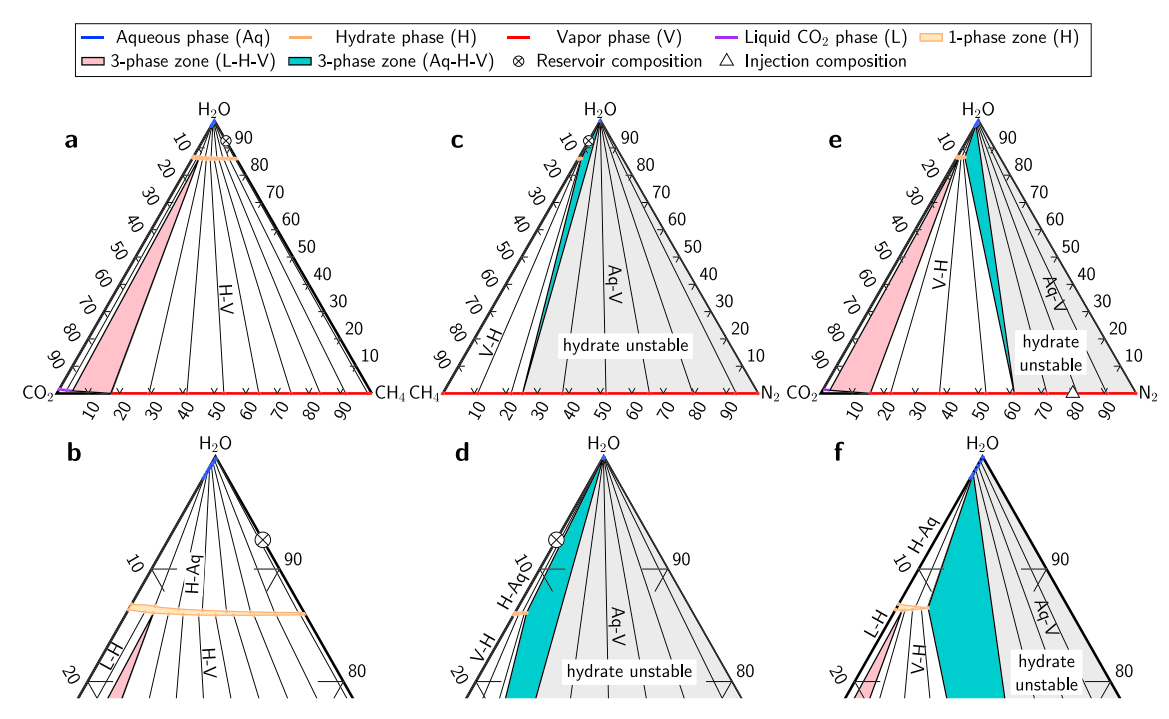


Figure 2. Ternary phase diagrams for (a and b) $H_2O/CH_4/CO_2$ mixtures, (c and d) $H_2O/CH_4/N_2$ mixtures, and (e and f) $H_2O/CO_2/N_2$ mixtures at $4^{\circ}C$, 50 bar, (black circle, Figure 1). Figures 2a, 2c, and 2e show the complete ternary diagram. Figures 2b, 2d, and 2f show the enlarged ternary diagrams near H_2O vertex. Mole percent of bottom right component, bottom left component, and H_2O are labeled along bottom, left, and right axes, respectively. Two-phase zones (e.g., H-V, Aq-H, and H-L) have tie lines connecting stable phases drawn with thin, black lines. Three-phase zones (L-H-V and Aq-H-V) are indicated by shaded tie triangles. A single-phase hydrate zone is shaded in orange. The two-phase zone Aq-V is shaded in gray. A hypothetical reservoir composition of 50 mol % of methane hydrate and 50 mol % fresh water is marked with a crossed circle, and an injection composition of 80 mol % N_2 and 20 mol % N_2 is marked with a white triangle.

phase diagrams (Figure 2), and compositional quaternary phase diagrams (Figures 3 and 4). We directly compare (Figure 4) a N_2 -rich injection to a CO_2 -rich injection and show that the emergence of three-phase equilibrium in N_2 -rich injections maintains two mobile phases in addition to the immobile hydrate phase. This allows phase-wise partitioning of the components where N_2 dissociates CH_4 hydrate and CO_2 forms mixed hydrate. Our findings fundamentally explain the role N_2 plays in the conflicting, ambiguous processes present during injection of N_2 and CO_2 mixtures into CH_4 hydrate-bearing sediment. We restrict our analysis to a fresh water system for simplicity, so these results are directly applicable to hydrate-forming, subpermafrost environments like the field site, Ignik Sikumi on Alaska's northern slope [Boswell et al., 2017]. However, these results are equally applicable to hydrate-forming saline systems since salt impacts hydrate stability through freezing point depression. Thus, our results hold for hydrate-based CO_2 storage in submarine environments where CH_4 hydrate is abundant [Boswell and Collett, 2011].

2. Methods

We simulate thermodynamic stability of mixed and simple hydrates using a flash-type computational framework [Sloan and Koh, 2007; A. Ballard and E. Sloan, 2004] coupled with equations of state that are accurate and suitable for hydrates [Ballard and Sloan, 2002; Jager et al., 2003]. We compare individual flash calculations to the thermodynamic simulator CSMGem [L. Ballard and E. Sloan, 2004] (Tables S2 and S3 in the supporting information), which was experimentally validated for H₂O/CH₄/CO₂/N₂ mixtures [Sun et al., 2016]. However, we cannot directly compare our ternary or quaternary diagrams with CSMGem because CSMGem does not have this capability. Small differences in the calculations potentially change minor things about the presented phase diagrams but would not eliminate the fundamental finding of three-phase equilibrium regions in the composition space.

We focus our analysis primarily on a single thermodynamic condition, 50 bar and 4°C (black circle, Figure 1) to describe the details of the phase diagrams. We simulate various other thermodynamic conditions (squares and diamonds, Figure 1) and present the variability of the phase diagrams as a function of pressure and



temperature (Figures S4 and S5). Our simulated thermodynamic conditions are comparable to the experimental conditions of other studies (cross marks, Figure 1) summarized in Table S1, including the field test at Ignik Sikumi [Schoderbek and Boswell, 2011; Boswell et al., 2017], on the northern slope of Alaska, U.S. (\approx 85 bar, \approx 4°C).

We consider the possibility of an aqueous phase (Aq), a vapor phase (V), a liquid CO_2 phase (L), and a hydrate phase (H). We restrict the calculation to temperatures above $0^{\circ}C$ (i.e., no ice phase) and consider only structure 1 hydrate.

These results apply to fresh water systems since we do not explicitly model the impact of salt on the phase diagrams. However, it is well known that salt impacts hydrate stability through freezing point depression, similar to the freezing of water. Thus, our results also apply to saline systems.

3. Results and Discussion

We present numerous phase diagrams at various thermodynamic conditions that span the pressure-temperate regime most relevant for hydrate-based CO_2 storage. At 50 bar and 4°C (black circle, Figure 1), we show ternary phase diagrams (Figure 2) where one of the four components is absent. At these conditions, simple (i.e., a single guest) CH_4 hydrate (brown line, Figure 1) and simple CO_2 hydrate (purple line, Figure 1) are stable, while simple N_2 hydrate (teal line, Figure 1) is not stable. Liquid CO_2 (dashed purple line, Figure 1) is stable but vaporizes when combined with sufficient N_2 and/or CH_4 . Hydrate stability curves for an infinite number of mixtures with these components could also be plotted. For reference, we show the stability curves for a 50 mol % CH_4 and 50 mol % CO_2 mixture (pink line, Figure 1) and an 80 mol % N_2 and 20 mol % CO_2 mixture (red line, Figure 1). We explore additional thermodynamic conditions (squares and diamonds, Figure 1) with ternary (Figures 2, S4, and S5) and quaternary (Figures 3, 4, and S4) phase diagrams.

3.1. Ternary Diagrams at 50 bar and 4°C

The ternary phase diagrams (Figure 2) show the compositionally dependent phase stabilities when one of the four components is absent. The aqueous (Aq) single-phase zone occurs near the H_2O vertices at compositions below the mixture solubility. The vapor (V) single-phase zone occurs near the H_2O -free ternary edge at compositions below the vapor saturation of H_2O . The liquid CO_2 (L) single-phase zone occurs near the CO_2 vertex.

In all ternary diagrams (Figure 2), an abrupt phase transition separates the hydrate-vapor (H-V) two-phase zone from the aqueous-hydrate (Aq-H) two-phase zone. This transition is visible in the blow up of the ternary diagrams (Figures 2b, d, and 2f) and occurs for both mixed and simple hydrates (e.g., along $\rm H_2O-CH_4$ ternary edge of Figure 2a). It is commonly referred to as the transition separating the excess-water zone (i.e., Aq-H zone) from the excess-gas zone (i.e., V-H zone). Between these two-phase zones, a single-phase hydrate zone (orange shaded area, Figure 2) is present such that the hydrate composition is identical to the overall composition.

Two distinct types of three-phase zones occur within these ternary diagrams. In the $\rm H_2O/CH_4/N_2$ (Figures 2c and 2d) and $\rm H_2O/CO_2/N_2$ (Figures 2e and 2f) ternary diagrams, an aqueous-hydrate-vapor (Aq-H-V) three-phase zone occurs near the middle of the ternary diagrams. The Aq-H-V zones separate the aqueous-vapor (Aq-V) two-phase zone from the hydrate stable zones. At low $\rm N_2$ abundance relative to the other guests hydrate is stable, while hydrate is not stable at high $\rm N_2$ abundance relative to the other guests (gray regions, Figure 2). In the $\rm H_2O/CH_4/CO_2$ (Figures 2a and 2b) and $\rm H_2O/CO_2/N_2$ (Figures 2e and 2f) ternary diagrams, a liquid-hydrate-vapor (L-H-V) three-phase zone occurs near the ternary edge connecting $\rm CO_2$ and $\rm H_2O$. This zone separates the liquid-hydrate (L-H) zone from the hydrate-vapor (H-V) zone. At high $\rm CO_2$ abundance relative to the other guests, liquid $\rm CO_2$ is stable, while vapor is stable at low $\rm CO_2$ abundance relative to the other guests.

3.2. Quaternary Diagrams at 50 bar and 4°C

The ternary diagrams (Figure 2) are equivalent to exterior faces of a larger quaternary diagram of the complete $H_2O/CH_4/CO_2/N_2$ system, so the information contained in the ternary diagrams can be extrapolated to the quaternary diagrams. We highlight the two most important features of the ternary diagrams: the hydrate unstable zone (gray zone, Figures 2c-2f) and the Aq-H-V three-phase zone (teal tie triangle, Figures 2c-2f). We show how these zones project onto the exterior of the quaternary diagram (Figure 3a) and extend through the interior of the quaternary diagram (Figures 3b-3d).

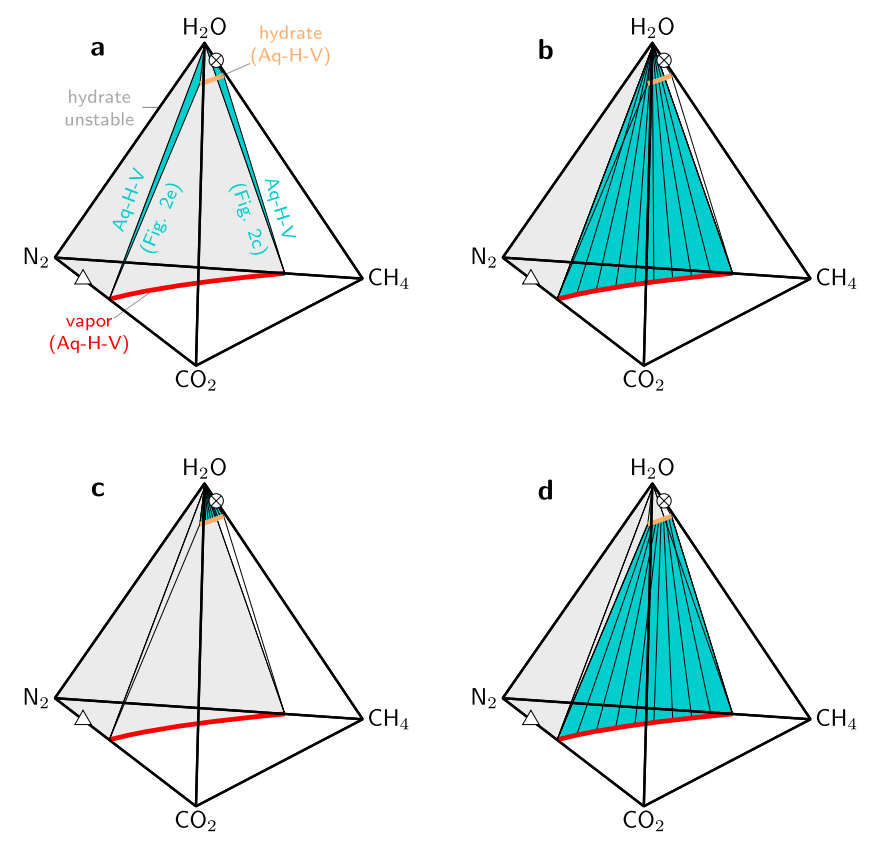


Figure 3. Quaternary phase diagrams for H₂O/CH₄/CO₂/N₂ mixtures at 4°C, 50 bar (black circle, Figure 1) with four different perspectives of teal-shaded Aq-H-V three-phase zone. Compositions inside the bounding surfaces of Aq-H-V zone are at three-phase equilibrium. Vapor (red line), hydrate (orange line), and aqueous (not drawn) compositions vary throughout the interior of three-phase zone. Hypothetical reservoir composition (crossed circle) and potential injection composition (white filled triangle) from Figure 2 are marked for reference. (a) Exterior faces of Aq-H-V zone shown in Figures 2c-2f shaded in teal. (b) Interior surface of Aq-H-V zone connecting vapor and aqueous phases shaded in teal. (c) Interior surface of Aq-H-V zone connecting hydrate and aqueous phases shaded in teal. (d) Interior surface of Aq-H-V zone connecting vapor and hydrate phases shaded in teal.

The Aq-H-V three-phase zone is not simply a tie triangle on the exterior faces, but instead a sequence of tie triangles that spans from the $H_2O/CH_4/N_2$ exterior face to the $H_2O/CO_2/N_2$ exterior face. The interior tie triangles have continuous composition variations in the aqueous, hydrate (orange line, Figures 3 and 4), and vapor phases (red line, Figures 3 and 4). The complete Aq-H-V three-phase zone within the quaternary diagram is a three-dimensional volume bounded by surfaces connecting the vapor and aqueous phases (teal surface, Figure 3b), the aqueous and hydrate phases (teal surface, Figure 3c), and the hydrate and vapor phases (teal surface, Figure 3d). Each surface of the Aq-H-V three-phase zone represents a family of tie triangle edges (thin, black lines Figure 3).

The one-, two-, and three-phase zones of the ternary diagrams are defined analogously in the quaternary diagram. Hydrate is unstable at compositions whose N_2 fraction exceeds the N_2 fraction on the surface of the Aq-H-V zone connecting the aqueous and vapor phases (gray zone, Figure 3), and compositions in this zone fall on tie lines connecting the aqueous and vapor phases. Three phases (Ag-H-V) are stable for compositions inside the Aq-H-V bounded volume, and each composition has a corresponding tie triangle that connects the three phases (thin, black lines on teal surfaces, Figure 3). Hydrate is unconditionally stable at compositions whose N₂ fraction does not exceed the N₂ fraction on any surface of the Aq-H-V three-phase zone. Hydrate stable compositions with a H₂O fraction below ≈86 mol % fall on tie lines in the H-V zone. Likewise, hydrate stable compositions with a H_2O fraction above \approx 86 mol % fall on tie lines in the Aq-H zone. Although not pictured, compositions near the CO₂ edge of the quaternary diagram form a liquid CO₂ phase. Thus, there are L, L-H, and L-H-V zones near the CO₂ edge that span the interior of the quaternary diagram between



the analogous zones of the exterior faces in the ternary diagrams. We exclude the liquid CO_2 zones from the quaternary diagram because they are not relevant for the rest of the discussion.

3.3. Injection Comparison

Our results show how variations in composition of a hydrate system containing N_2 lead to changes in phase stability and the potential for three-phase equilibrium. These results illuminate how the dual function of N_2 as a hydrate inhibitor at high abundance and a hydrate former at low abundance combine to produce a Aq-H-V three-phase equilibrium zone. Previous work suggests that N_2 is either a hydrate inhibitor [Panter et al., 2011] or a hydrate former [Youn et al., 2016; Park et al., 2006], not both. Yet laboratory results [Birkedal et al., 2015; Kang et al., 2014] and the Ignik Sikumi field test [Schoderbek and Boswell, 2011; Hauge et al., 2014; Boswell et al., 2017] hinted that the system evolved in a more complex way than this mutually exclusive binary categorization. Simulations of hydrate exchange at Ignik Sikumi [White and Suk Lee, 2014; Anderson et al., 2014; Hauge et al., 2014] may demonstrate three-phase stability; however, neither the simulations [Anderson et al., 2014] nor the thermodynamic underpinning [Garapati and Anderson, 2014] directly addresses three-phase equilibrium. Furthermore, pseudoternary diagrams of the $H_2O/CH_4/CO_2/N_2$ system [Garapati and Anderson, 2014] suggest that only Aq-H or H-V two-phase stability is possible.

Our analysis explains how phase stability is impacted by overall mixture composition, but gas injections are dynamic processes in which local compositions constantly change due to the flow of one or more phases [Anderson et al., 2014; Youn et al., 2016]. Enhanced oil recovery is another dynamic injection process that couples multiphase flow with phase behavior and is often modeled with the aid of a graphical visualization to analyze the evolution of the reservoir [Orr, 2007]. Here we borrow the graphical techniques of enhanced oil recovery to understand the first-order response of gas injections into CH_4 hydrate reservoirs. In particular, we compare injections rich in CO_2 (J_1 , Figure 4a) with those rich in N_2 (J_2 , Figure 4b). We use the graphical analysis to show how phases stabilities change (area plots, Figure 4) when either injection is linearly combined with a hypothetical reservoir composition (I, Figure 4) along a mixing line connecting the injections to the reservoir (J_1 -I and J_2 -I, Figure 4). Along each mixing line, the compositions of each stable phase also change (line plots, Figure 4), which has implications for the transport of each component.

The $\mathrm{CO_2}$ -rich injection (J_1 -I, Figure 4a) is initially a single-phase vapor, but small increases in $\mathrm{H_2O}$ fraction form hydrate in the two-phase H-V zone (yellow portion of mixing line, Figure 4a). Along the mixing line from J_1 to I, the $\mathrm{H_2O}$ fraction increases and more hydrate forms within the two-phase H-V zone (area plot, Figure 4a). When the $\mathrm{H_2O}$ fraction exceeds the $\mathrm{H_2O}$ fraction within the hydrate phase, the mixing line abruptly transitions into a two-phase Aq-H zone (black portion of mixing line, Figure 4a). Thus, all compositions along the mixing line are hydrate stable with excess material in only one other phase. This is characteristic of the current conceptual picture for guest molecule exchange. In this type of injection, the injected gas forms mixed hydrate whose composition is different than the initial $\mathrm{CH_4}$ hydrate, but the injection does not induce hydrate dissociation. We suspect that these type of injections are solid-solid, diffusion-based transport processes [Ota et al., 2005b]. Furthermore, the constant hydrate stability along the mixing line might lead to plugging of the reservoir as the injected material forms hydrate with $\mathrm{H_2O}$ initially in the pore space, eventually restricting fluid flow.

Conversely, the N_2 -rich injection (J_2 -I, Figure 4b) is initially a single-phase vapor and does not form hydrate when the H₂O fraction is moderately increased. Instead, mixtures with small H₂O fractions are located in the two-phase Aq-V zone (gray portion of mixing line, Figure 4b). Mixtures with a substantial H₂O fraction are in the three-phase Aq-H-V zone (teal portion of mixing line, Figure 4b), and mixtures with large H₂O fraction are in the two-phase Aq-H zone (black portion of mixing line, Figure 4b). This means that the injected composition could dissociate the initial CH₄ hydrate or form mixed hydrate depending on the local mixture. In addition, most mixtures along the mixing line have aqueous and vapor phase stabilities, so two-phase flow is possible. Therefore, the local mixtures will constantly change as the flowing phases move downstream at different speeds and with different compositions. The difference in compositions between the vapor and hydrate phases (line plots, Figure 4b) will have a significant impact on the internal dynamics of the reservoir, since the vapor and aqueous phases are mobile, but the hydrate phase is not. Based on this analysis, CO₂ (dash dotted line plots, Figure 4b) preferentially enters the hydrate phase and, thus, slowly penetrates the reservoir because hydrate is immobile. In addition, N₂ (solid-line plots, Figure 4b) preferentially enters the vapor phase, and thus, quickly penetrates the reservoir due to the high mobility of the vapor phase. At three-phase equilibrium (teal portion of mixing line, Figure 4b), CH₄ (dashed-line plots, Figure 4b) and N₂ (solid-line plots, Figure 4b) enrich the vapor phase, while CO_2 (dot-dashed-line plots, Figure 4b) enriches the hydrate and aqueous phases.

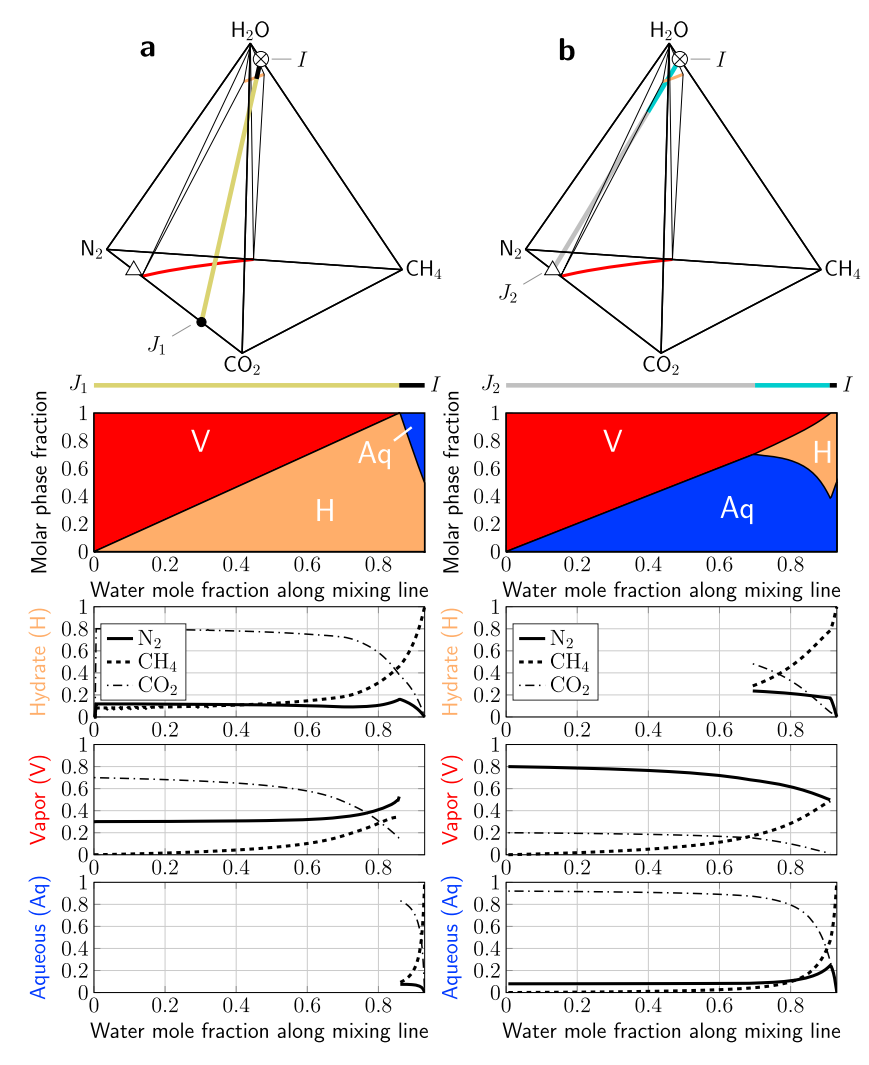


Figure 4. Comparison of injections at 4°C, 70 bar (blue square, Figure 1). Quaternary diagrams show mixing lines (J_1-I,J_2-I) that linearly connect injections to a hypothetical reservoir composition I (93/07 mol % (H₂O/CH₄)). Shaded plots show molar phase fraction as a function of H₂O mole fraction. Line plots show phase wise, guest-only composition as a function H_2O mole fraction. (a) CO_2 -rich injection (30/70 mol % $(N_2/CO_2))$ J_1 is a vapor phase. Yellow portion of mixing line J_1 -I is in the H-V two-phase zone, and black portion (above 86 mol % H_2O) is in the Aq-H two-phase zone. (b) N_2 -rich injection (80/20 mol % (N_2 /CO₂)) J_2 is a vapor phase. Gray portion of mixing line J_2 -I is hydrate unstable (Aq-V), teal portion is at three-phase equilibrium (Aq-H-V), and black portion is hydrate stable (Aq-H).

This phase-wise fractionation may lead to highly mobile, N_2 -rich vapor that dissociates the initial CH_4 hydrate deep into the reservoir, while most of the injected CO₂ forms immobile, mixed hydrate close to the injection. We surmise that these type of injections are the types that maintain injectivity (i.e., prevent plugging) [Birkedal et al., 2015] and allow for a combination of guest molecule exchange and hydrate dissociation [Kang et al., 2014; Boswell et al., 2017] that has been called a bulk exchange [Boswell et al., 2017]. Therefore, the mechanism responsible for the improved efficiency of flue gas injections compared to CO₂-rich injections is the partitioning into hydrate stable/unstable zones, which transports each component through the reservoir at different speeds and in different phases.

A dynamic analysis that includes fluid flow would likely show that the injection and reservoir compositions do not connect linearly but instead connect along a complicated nonlinear path. This type of analysis is beyond the scope of this work; however, extensive gas injection analyses [Orr, 2007] indicate that the linear mixing/dilution line provides a first-order approximation to the phase stability and flow behavior of reservoir injections.



4. Implications and Other Applications

Our injection comparison suggests there may be optimal conditions for storage of CO_2 as hydrate and/or production of CH_4 hydrates. Optimal CO_2 storage occurs when the injection mixture is at or near three-phase equilibrium. Such mixtures avoid excessive hydrate buildup near the injection and also store CO_2 in the aqueous and hydrate phases. The amount of mixed CO_2 hydrate formation depends on the local mixture everywhere within the reservoir, which is impacted by fluid and heat flow in addition to the reservoir characteristics. Optimal CH_4 hydrate production occurs when the injection is very unstable to hydrate formation such as pure N_2 , N_2 -rich mixtures of N_2 and CO_2 , or air [Kang et al., 2014]. While most studies of injections at hydrate-forming conditions focus on simultaneous storage of CO_2 as hydrate and production of CH_4 hydrates (i.e., "guest molecule exchange"), our work implies that the maximum exchange of guests may be a two-stage process. In stage one, pure N_2 injection produces methane hydrates (i.e. "nitrogen-induced production"). In stage two, coinjection of N_2 and CO_2 stores CO_2 in hydrates (i.e. "nitrogen-assisted storage"). We outline these individual processes below.

4.1. Nitrogen-Induced Production

Methane hydrate production by N_2 injection likely behaves similarly to the injections of N_2 and CO_2 mixtures we presented, but with more dissociation and less exchange. While one appeal of guest molecule exchange for CH_4 hydrate production is that it maintains structural integrity of the reservoir during production, it is not clear that a reservoir will actually collapse due to rapid dissociation from any production technique [*Terao et al.*, 2014]. Therefore, it is reasonable to directly inject a cheap hydrate inhibitor, such as N_2 , to produce hydrate and bypass the exchange process altogether. Our analysis shows that mixed hydrate may still form, which could provide more structural integrity during production than would occur from depressurization alone. In addition, laboratory experiments of nitrogen purging in hydrate-plugged pipelines already show that N_2 injection is an efficient technique for hydrate dissociation [*Panter et al.*, 2011], so it would likely perform equally well in natural reservoirs.

4.2. Nitrogen-Assisted Storage

 CO_2 storage as hydrate is possible without CH_4 hydrate production [House et al., 2006; Rochelle et al., 2009; You et al., 2015] in various marine and arctic settings due to the favorable thermodynamic conditions for CO_2 hydrate formation. The limiting factor on CO_2 storage as hydrate is the possibility of excessive hydrate buildup [House et al., 2006] near the injection or anywhere else within the reservoir. An efficient technique for CO_2 storage would need to deal with this issue by sufficiently limiting CO_2 hydrate formation. Our analysis shows that CO_2 acts as a hydrate inhibitor that buffers hydrate formation, so flue gas injection into fresh or saline water may avoid the plugging issues associated with hydrate-based pure CO_2 storage. This type of storage could be applied in reservoirs first depleted in CCO_3 hydrate by any production technique or in aquifers at hydrate-forming conditions.

5. Conclusion

Our results show that three-phase equilibrium is a prevalent feature of hydrate systems that include N₂ at thermodynamic conditions unfavorable to simple N₂ hydrate stability. This type of three-phase equilibrium demonstrates that even at fixed temperature and pressure, N2 behaves as a hydrate-inhibiting substance, as well as a hydrate-forming substance depending on its relative abundance. Furthermore, the three-phase equilibrium conditions that occur in hydrate systems consisting of H₂O/CH₄/CO₂/N₂ mixtures are likely the reason that injections of N_2 and CO_2 mixtures (i.e., flue gas) have successfully produced CH_4 hydrate and stored CO_2 as hydrate in the lab and in the field through a bulk exchange. Injections rich in N_2 combine mixed hydrate formation with hydrate dissociation thereby limiting massive hydrate formation that otherwise causes plugging. Injections of this type contrast with pure CO₂ and CO₂-rich injections in which hydrate formation will approach 100% saturation, if sufficient water is available. Since injection composition significantly impacts phases stabilities, results from one injection composition cannot be applied to another injection composition without a phase behavior analysis. An optimal strategy for combined CO_2 storage as hydrate and CH_4 hydrate production may be a two-stage process. In stage one, injection of pure N2 or air into CH4 hydrate-bearing reservoirs produces all CH_4 in the reservoir through dissociation. In stage two, injection of flue gas, which is at or near three-phase equilibrium, into the CH₄-depleted reservoir stores CO₂ in the reservoir within all stable phases including hydrate, while limiting hydrate formation near the injection.



Our results apply to all environments with hydrate-forming thermodynamic conditions, such as subpermafrost and submarine CH₄ hydrate-bearing reservoirs. Further heat and flow modeling work is required to understand the specific partitioning that occurs during hydrate-related gas injection processes. While this work is directly related to hydrate-based exchange by flue gas injection, the implications of multiphase stability may be applicable to other mixed hydrate systems.

Acknowledgments

This work was funded by DOE grant DE-FE0010406. Comparison of our calculations with CSMGem is in the supporting information file. Flash calculation code is available for download at https://github.com/kdarnell/ hydrateflash.

References

- Anderson, B., R. Boswell, T. S. Collett, H. Farrell, S. Ohtsuki, M. White, and M. Zyrianova (2014), Review of the findings of the liquik sikumi CO₂-CH₄ gas hydrate exchange field trial, paper presented at the 8th International Conference on Gas Hydrates (ICGH8-2014), ICGH, Beijing, China, 28 Jul. - 1 Aug.
- Ballard, A., and E. Sloan (2004), The next generation of hydrate prediction: Part III. Gibbs energy minimization formalism, Fluid Phase Equilibria, 218(1), 15-31.
- Ballard, A., and E. Sloan Jr. (2002), The next generation of hydrate prediction: I. Hydrate standard states and incorporation of spectroscopy, Fluid Phase Equilibria, 194, 371-383.
- Ballard, L., and E. Sloan (2004), The next generation of hydrate prediction IV: A comparison of available hydrate prediction programs, Fluid Phase Equilibria, 216(2), 257-270.
- Birkedal, A. K., P. L. Hauge, A. Graue, and G. Ersland (2015), Transport mechanisms for CO2-CH₄ exchange and safe CO₂ storage in hydrate-bearing sandstone, Energies, 8(5), 4073-4095, doi:10.3390/en8054073.
- Boswell, R. (2007), Resource potential of methane hydrate coming into focus, J. Pet. Sci. Eng., 56(1-3), 9-13, doi:10.1016/i.petrol.2006.09.002.
- Boswell, R., and T. S. Collett (2011), Current perspectives on gas hydrate resources, Energy Environ. Sci., 4(4), 1206-1215.
- Boswell, R., D. Schoderbek, T. S. Collett, S. Ohtsuki, M. White, and B. J. Anderson (2017), The ignik sikumi field experiment, Alaska North Slope: Design, operations, and implications for CO₂-CH₄ exchange in gas hydrate reservoirs, Energy Fuels, 31(1), 140-153, doi:10.1021/acs.energyfuels.6b01909.
- Collett, T. S., R. Boswell, M. W. Lee, B. J. Anderson, K. Rose, and K. A. Lewis (2012), Evaluation of long-term gas-hydrate-production testing locations on the Alaska North Slope, Soc. Pet. Eng., 15(2), 243-264, doi:10.2118/155504-PA.
- Garapati, N., and B. J. Anderson (2014), Statistical thermodynamics model and empirical correlations for predicting mixed hydrate phase equilibria, Fluid Phase Equilibria, 373, 20-28, doi:10.1016/j.fluid.2014.03.010.
- Graue, A., B. Kvamme, B. Baldwin, J. Stevens, J. J. Howard, E. Aspenes, G. Ersland, J. Husebo, and D. Zornes (2008), Mri visualization of spontaneous methane production from hydrates in sandstone core plugs when exposed to CO₂, Soc. Pet. Eng., 13(2), 146–152, doi:10.2118/118851-PA.
- Hauge, L., K. Birkedal, G. Ersland, and A. Graue (2014), Methane production from natural gas hydrates by CO₂ replacement-review of lab experiments and field trial, in SPE Bergen One Day Seminar, pp. 1-12, Soc. Pet. Eng., Bergen, Norway.
- House, K. Z., D. P. Schrag, C. F. Harvey, and K. S. Lackner (2006), Permanent carbon dioxide storage in deep-sea sediments, Proc. Natl. Acad. Sci., 103(33), 12,291 – 12,295, doi:10.1073/pnas.0605318103.
- Jager, M., A. Ballard, and E. Sloan (2003), The next generation of hydrate prediction: II. Dedicated aqueous phase fugacity model for hydrate prediction, Fluid Phase Equilibria, 211(1), 85-107.
- Kang, H., D.-Y. Koh, and H. Lee (2014), Nondestructive natural gas hydrate recovery driven by air and carbon dioxide, Sci. Rep., 4, 6616.
- Koh, D.-Y., H. Kang, D.-O. Kim, J. Park, M. Cha, and H. Lee (2012), Recovery of methane from gas hydrates intercalated within natural sediments using CO₂ and a CO₂/N₂ gas mixture, ChemSusChem, 5(8), 1443-1448, doi:10.1002/cssc.201100644.
- Lee, H., Y. Seo, Y. Seo, I. L. Moudrakovski, and J. A. Ripmeester (2003), Recovering methane from solid methane hydrate with carbon dioxide, Angewandte Chemie Int. Edn., 42(41), 5048-5051.
- Lee, S., Y. Lee, J. Lee, H. Lee, and Y. Seo (2013), Experimental verification of methane-carbon dioxide replacement in natural gas hydrates using a differential scanning calorimeter, Environ. Sci. Technol., 47(22), 13,184-13,190, doi:10.1021/es403542z.
- Milkov, A. V. (2004), Global estimates of hydrate-bound gas in marine sediments: How much is really out there?, Earth Sci. Rev., 66(3),
- Moridis, G. J., and M. T. Reagan (2011), Estimating the upper limit of gas production from class 2 hydrate accumulations in the permafrost: 1. Concepts, system description, and the production base case, J. Pet. Sci. Eng., 76(3-4), 194-204, doi:10.1016/j.petrol.2010.11.023.
- Moridis, G. J., M. B. Kowalsky, and K. Pruess (2007), Depressurization-induced gas production from class-1 hydrate deposits, SPE Reservoir Eval. Eng., 10(5), 458-481.
- Ohgaki, K., K. Takano, H. Sangawa, T. Matsubara, and S. Nakano (1996), Methane exploitation by carbon dioxide from gas hydrates—Phase equilibria for CO₂-CH₄ mixed hydrate system, J. Chem. Eng. Jpn., 29(3), 478-483.
- Orr, F. M. (2007), Theory of Gas Injection Processes, Tie-Line Publ., Denmark.
- Ota, M., K. Morohashi, Y. Abe, M. Watanabe, R. Smith, and H. Inomata (2005a), Replacement of CH₄ in the hydrate by use of liquid CO₂, Energy Conv. Manag., 46, 1680-1691.
- Ota, M., Y. Abe, M. Watanabe, R. L. Smith Jr., and H. Inomata (2005b), Methane recovery from methane hydrate using pressurized CO₂, Fluid Phase Equilibria, 22-229, 553 – 559, doi:10.1016/j.fluid.2004.10.002, {PPEPPD} 2004 Proceedings
- Paganoni, M., J. Cartwright, M. Foschi, R. Shipp, and P. Van Rensbergen (2016), Structure II gas hydrates found below the bottom-simulating reflector, Geophys. Res. Lett., 43, 5696-5706, doi:10.1002/2016GL069452.
- Panter, J. L., A. L. Ballard, A. K. Sum, E. D. Sloan, and C. A. Koh (2011), Hydrate plug dissociation via nitrogen purge: Experiments and modeling, Energy Fuels, 25(6), 2572-2578, doi:10.1021/ef200196z.
- Park, Y., D.-Y. Kim, J.-W. Lee, D.-G. Huh, K.-P. Park, J. Lee, and H. Lee (2006), Sequestering carbon dioxide into complex structures of naturally occurring gas hydrates, Proc. Natl. Acad. Sci., 103(34), 12,690-12,694, doi:10.1073/pnas.0602251103.
- Rochelle, C. A., A. P. Camps, D. Long, A. Milodowski, K. Bateman, D. Gunn, P. Jackson, M. A. Lovell, and J. Rees (2009), Can CO₂ hydrate assist in the underground storage of carbon dioxide?, Geol. Soc. London Spec. Publ., 319(1), 171 – 183, doi:10.1144/sp319.14.
- Schoderbek, D., and R. Boswell (2011), Ignik Sikumi 1, gas hydrate test well, successfully installed on the Alaska North Slope, Nat. Gas Oil,
- Seo, Y.-j., D. Kim, D.-Y. Koh, J. Y. Lee, T. Ahn, S.-J. Kim, J. Lee, and H. Lee (2015), Soaking process for the enhanced methane recovery of gas hydrates via CO₂/N₂ gas injection, Energy Fuels, 29(12), 8143-8150, doi:10.1021/acs.energyfuels.5b02128.
- Sloan, E. D., Jr., and C. Koh (2007), Clathrate Hydrates of Natural Gases, CRC Press, New York.



- Smith, A. J., J. Mienert, S. Bünz, and J. Greinert (2014), Thermogenic methane injection via bubble transport into the upper Arctic Ocean from the hydrate-charged Vestnesa Ridge, Svalbard, *Geochem. Geophys. Geosyst.*, 15, 1945–1959.
- Sun, D., and P. Englezos (2017), Determination of CO₂ storage density in a partially water-saturated lab reservoir containing CH₄ from injection of captured flue gas by gas hydrate crystallization, *Can. J. Chem. Eng.*, 95(1), 69–76, doi:10.1002/cjce.22655.
- Sun, D., J. Ripmeester, and P. Englezos (2016), Phase equilibria for the CO₂/CH₄/N₂/H₂O system in the hydrate region under conditions relevant to storage of CO₂ in depleted natural gas reservoirs, *J. Chem. Eng. Data*, 61(12), 4061–4067, doi:10.1021/acs.jced.6b00547.
- Swart, P. K., U. Wortmann, R. Mitterer, M. Malone, P. Smart, D. Feary, and A. Hine (2000), Hydrogen sulfide-hydrates and saline fluids in the continental margin of South Australia, *Geology*, 28(11), 1039–1042.
- Terao, Y., M. Duncan, B. Hay, and L. Dang (2014), Deepwater methane hydrate gravel packing completion results and challenges, paper presented at Offshore Technology Conference, Houston, Tex., 5–8 May.
- Wallmann, K., E. Pinero, E. Burwicz, M. Haeckel, C. Hensen, A. Dale, and L. Ruepke (2012), The global inventory of methane hydrate in marine sediments: A theoretical approach, *Energies*, 5(7), 2449–2498.
- White, M., and W. Suk Lee (2014), Guest molecule exchange kinetics for the 2012 Ignik Sikumi gas hydrate field trial, paper presented at Offshore Technology Conference, Houston, Tex., 5–8 May.
- Yonkofski, C. M., J. A. Horner, and M. D. White (2016), Experimental and numerical investigation of hydrate-guest molecule exchange kinetics, J. Nat. Gas Sci. Eng., 35, 1480 1489.
- You, K., D. DiCarlo, and P. B. Flemings (2015), Quantifying hydrate solidification front advancing using method of characteristics, *J. Geophys. Res. Solid Earth*, 120, 6681 6697, doi:10.1002/2015JB011985.
- Youn, Y., M. Cha, M. Kwon, J. Park, Y. Seo, and H. Lee (2016), One-dimensional approaches for methane hydrate production by CO₂/N₂ gas mixture in horizontal and vertical column reactor, *Korean J. Chem. Eng.*, 33(5), 1712–1719, doi:10.1007/s11814-015-0294-5.